Journal of Applied Fluid Mechanics, Vol. 10, No. 3, pp. 847-859, 2017.
Available online at www.jafmonline.net, ISSN 1735-3572, EISSN 1735-3645.
DOI: 10.18869/acadpub.jafm.73.240.26388

Analysis of Turbulent Natural Convection by an Elliptic Relaxation Model in Tall Vertical Cavities with Linear Temperatures on Sidewalls

L. El Moutaouakil, Z. Zrikem† and A. Abdelbaki

Cadi Ayyad University, Faculty of Sciences Semlalia (LMFE), BP 2390, Marrakech 40000, Morocco

†*Corresponding Author Email: zrikem@uca.ac.ma, zrikem@uca.ma*

(Received April 9, 2016; accepted January 3, 2017)

ABSTRACT

Turbulent natural convection of air is studied, by the elliptic-relaxation model v^2-f, in a tall vertical cavity whose hot and cold walls are maintained at linear temperatures of slopes γ_1 and γ_2, respectively. The average temperatures of the active walls are located at mid-height of the cavity. Four situations are analyzed, corresponding to $\gamma_1=\gamma_2=\gamma$ (case I), $\gamma_1=-\gamma_2=\gamma$ (case II), $\gamma_1=0$ and $\gamma_2=\gamma$ (case III), $\gamma_1=\gamma$ and $\gamma_2=0$ (case IV). These boundary conditions may be more representative or used to control heat transfer for certain systems. The effects of the slope ($-1\leq\gamma\leq 1$), the aspect ratio of the cavity ($10\leq A\leq 80$) and the average Rayleigh number ($5\times10^4\leq Ra_m\leq10^6$) on the streamlines, isotherms, contours of the turbulent kinetic energy, heatlines, local and average Nusselt numbers are investigated. It is shown that the local and average heat transfers of cases III and IV can be deducted from those of cases I and II. The obtained dynamic and thermal fields as well as local and average heat transfers of the studied cases are quite different of those of the classical case corresponding to $\gamma=0$. A simplified procedure for calculating the average Nusselt number is also developed for each case.

Keywords: Turbulent natural convection; Tall vertical cavity; Linear temperature; v^2-f model; Heatlines; Simplified calculation tool.

NOMENCLATURE

A	aspect ratio
g	acceleration due to gravity
H	height of the cavity, m
k	turbulent kinetic energy
k_t	thermal conductivity
L	width of the cavity
	length scale of turbulence
Nu	Nusselt number
P	pressure
P_k	turbulent kinetic energy production
Pr	Prandtl number
Ra	Rayleigh number
t	fluctuating temperature component
T	mean temperature
	time scale of turbulence
u	fluctuating velocity component
U	mean velocity
$\overline{v^2}$	wall-normal Reynolds stress
x,y	horizontal and vertical coordinates
X,Y	dimensionless coordinates
α	thermal diffisuvity
β	thermal expansion coefficient
γ	slope of linear temperature profile
δ	Kronecker symbol
ΔT	temperature difference
ε	dissipation rate
θ	dimensionless temperature
ν	kinematic viscosity
ρ	density
τ	time
ψ	stream function
ω	specific dissipation rate

Subscripts

0	reference
1	hot wall
2	cold wall
c	cold, convection
h	hot
i,j	directions
L	local
m	mean
max	maximum
t	turbulent

1. INTRODUCTION

Several works have focused on turbulent natural convection in differentially heated cavities with uniform temperatures because of their importance in many practical applications (building elements, solar systems, electronic cooling). These works include those of Manz (2003), Xàman *et al.* (2005) and El Moutaouakil *et al.* (2015) who used the $k-\varepsilon\ HRN$ (high Reynolds number), $k-\varepsilon\ LRN$ (low Reynolds number) and $k-\omega\ SST$ (shear stress transport) turbulence models, respectively. Overall, the objective of these studies is to determine the flow structure and the convective heat transfer in vertical cavities filled with air and of an aspect ratio $A=4$ to 80. Nusselt numbers calculated numerically by Manz (2003) were compared with those estimated by some widely used correlations (Yin *et al.* 1978; ElSherbiny *et al.* 1982; Wright 1996; Zhao *et al.* 1997). While the results of Xàman *et al.* (2005) have been exploited to develop, in laminar and turbulent regimes for each A (20, 40, and 80), simple empirical expressions giving the average Nusselt number as a function of the Rayleigh number. However, the correlations developed by El Moutaouakil *et al.* (2015) in both flow regimes are more general since they take into account the aspect ratio of the cavity ($10 \le A \le 80$). It was observed that there are some differences between the results of these studies which are mainly due to the use of different turbulence models.

Indeed, for a turbulent flow in a given configuration, the precision of the numerical results depends on the used turbulence model. For this, several works have been devoted to the development and testing of turbulence models in order to identify the most appropriate one to a given situation (Zhang *et al.* 2007; Billard 2011; Aksouh *et al.* 2011; Rajani *et al.* 2012; El Moutaouakil *et al.* 2014a; Omranian *et al.* 2014). For engineering problems, it is well known that RANS (Reynolds averaged Navier–Stokes) models based on the turbulent viscosity (eddy-viscosity models) are among the easiest to implement while being efficient (El Moutaouakil *et al.* (2014a)). For tall cavities with differentially heated vertical walls by uniform temperatures, twenty eddy-viscosity models (EVM) with one-, two- or three-equation closure were tested recently by El Moutaouakil *et al.* (2014a). After comparing the numerical results with those experimental of Betts and Bokhari (2000), it was concluded that the elliptic-relaxation models have the best performance because they produce accurate results in a reasonable computing time.

Despite their importance to control the heat transfer or to get closer to real operating conditions of certain systems, there are few studies on cavities subjected to non-uniform temperatures. Published works in the literature concern mainly the laminar flows in cavities with weak aspect ratios ($A<10$) (Roy and Basak 2005; Basak *et al.* 2006; Saeid and Yaacob 2006; Sathiyamoorthy *et al.* 2007; Deng and Chang 2008; Basak *et al.* 2011; Aswatha *et al.* 2011; Aswatha *et al.* 2012; Anandalakshmi and Basak 2013) or with a high value of A ($A=40$) (El Moutaouakil *et al.* (2014b)). Overall, the objective of these works is to study the effect of non-uniform boundary conditions and control parameters on the flow and convective heat transfer characteristics in the cavity.

Thus, for tall vertical cavities, only the study of El Moutaouakil *et al.* (2014b) has treated in laminar regime the case of a cavity with $A=40$, whose horizontal walls are adiabatic while those vertical are subjected to linear temperature profiles. The average temperatures of the hot and cold walls are located at mid-height of the cavity and are used to calculate the average Rayleigh number Ra_m. This work has shown that the convective heat transfers as well as the primary and secondary flow structures depend strongly on the temperature profiles imposed on the hot and cold walls.

For sufficiently high values of Ra_m, the natural flow in tall vertical cavities becomes turbulent whatever the slopes γ_1 and γ_2 of the linear temperature profiles imposed on the hot and cold walls, respectively. For this purpose, the present work is dedicated to the study of turbulent natural convection ($5.10^4 \le Ra_m \le 10^6$) in tall vertical cavities ($10 \le A \le 80$) with different combinations of the slopes γ_1 and γ_2. Four situations are considered, corresponding to $\gamma_1=\gamma_2=\gamma$ (case I), $\gamma_1=-\gamma_2=\gamma$ (case II), $\gamma_1=0$ and $\gamma_2=\gamma$ (case III), $\gamma_1=\gamma$ and $\gamma_2=0$ (case IV) with $-1\le\gamma\le 1$.

To conduct this study, the three-equation turbulence model v^2-f of Hanjalic *et al.* (2004) has been implemented in a computer code that was developed and adapted to the considered configurations ($\gamma=-1, 0$ or 1). After the validation of the numerical code, a study is carried out on the effect of different linear temperature profiles on the characteristics of the turbulent natural flow and convective heat transfer within tall vertical cavities. In order to better visualize the convective heat transport, the concept of heatlines developed by Kimura and Bejan (1983) is used. This concept has been widely exploited mainly in laminar regime (Costa 2003; Basak *et al.* 2009; Kaluri *et al.* 2010; Basak *et al.* 2011; Ramakrishna *et al.* 2012; Basak and Chamkha 2012; Basak *et al.* 2013, Jamai *et al.* 2014; Arani *et al.* 2014). Finally, to facilitate the calculation of the average convective Nusselt number Nu_C as a function of the controlling parameters Ra_m and A, a simple procedure is developed for each of the slopes γ ($\gamma=-1,\ 0$ or 1) of every case considered (cases I to IV).

2. MATHEMATICAL FORMULATION

The studied two-dimensional tall vertical cavity and the considered thermal boundary conditions are shown in Figs. 1*a* and 1b. The width L and height H of the cavity are varied so that $10 \le A=H/L \le 80$. The horizontal walls are adiabatic while the dimensionless temperatures $\theta_i(Y)$ of the hot ($i=1$) and cold ($i=2$) walls vary linearly as a function of the height Y with a slope $\gamma_i=-1,0$ or 1 ($\theta_i(Y)=(T_i(y)-T_c)/(T_h-T_c)=\gamma_i(Y/A-0.5)+\delta_{i1}$, where $T_h=T_1(H/2)$ and $T_c=T_2(H/2)$). The

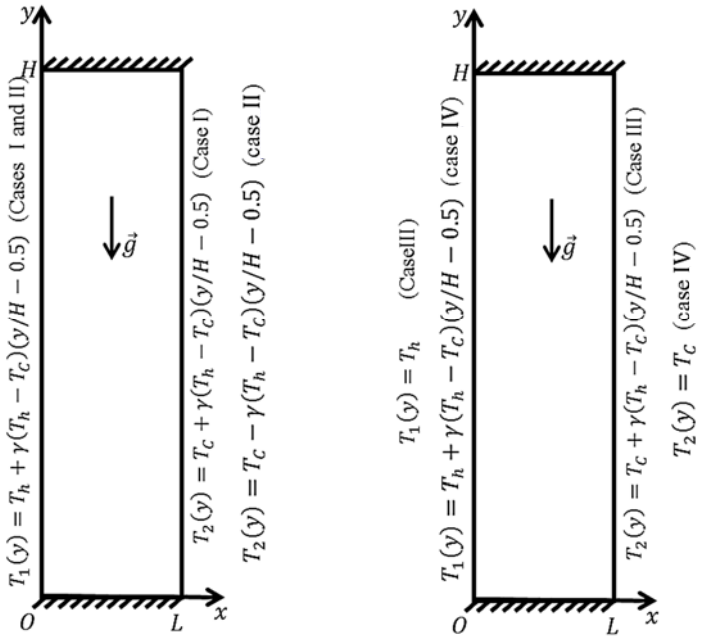

Fig. 1. Studied cases: a) cases I and II, and b) cases III and IV.

average temperature of each active wall is located at $Y = A/2$ and when $\gamma_i = 0$, the temperature of the wall i is uniform. The thermophysical properties of air are assumed to be constant ($Pr = 0.71$) except for the density in the buoyancy term for which the Boussinesq approximation is adopted.

The situations considered in this work are the cases I ($\gamma_1 = \gamma_2 = \gamma$) (Fig. 1a), II ($\gamma_1 = -\gamma_2 = \gamma$) (Fig. 1a), III ($\gamma_i = \delta_{i2}\gamma$) (Fig. 1b) and IV ($\gamma_i = \delta_{i1}\gamma$) (Fig. 1b). For case I, the slopes of the temperatures$\theta_1(Y)$ and $\theta_2(Y)$ are identical, hence their average $\theta_m(Y)$varies linearly with the height Y ($\theta_m(Y) = 0.5\big(\theta_1(Y) + \theta_2(Y)\big)$). By cons for case II, the slopes are equal but opposite which leads to a local Rayleigh number $Ra(Y)$ which varies with Y ($Ra(Y) = g\beta\big(T_1(y) - T_2(y)\big)L^3/\nu\alpha = Ra_m\big(\theta_1(Y) - \theta_2(Y)\big)$ with $Ra_m = Ra(Y = A/2) = g\beta(T_h - T_c)L^3/\nu\alpha$). For the last two cases III ($\gamma_1 = 0$) and IV ($\gamma_2 = 0$) , one of the two slopes is null, hence the quantities $\theta_m(Y)$ and $Ra(Y)$ vary simultaneously.

For turbulent natural convection within the cavity, the dimensionless governing equations for conservation of mass, momentum and energy are given by:

$$\frac{D\rho}{D\tau} \tag{1}$$

$$\frac{DU_i}{D\tau} = -\frac{1}{\rho}\frac{\partial P}{\partial x_i} + \frac{\partial}{\partial x_j}\left[2\nu S_{ij} - \overline{u_i u_j}\right] - g_i\beta(T - T_0) \tag{2}$$

$$\frac{DT}{D\tau} = \frac{\partial}{\partial x_j}\left[\frac{\nu}{Pr}\frac{\partial T}{\partial x_j} - \overline{u_j t}\right] \tag{3}$$

where $T_0 = (T_h + T_c)/2$

The Reynolds stresses $\overline{u_i u_j}$ and turbulent heat fluxes $\overline{u_j t}$ are expressed as a function of the mean dynamic and thermal quantities as follows.

$$\overline{u_i u_j} = \frac{2}{3}\delta_{ij}k - 2\nu_t S_{ij} \tag{4}$$

$$\overline{u_j t} = -\frac{\nu_t}{Pr_t}\frac{\partial T}{\partial x_j} \tag{5}$$

The strain-rate tensor and the turbulent viscosity are given by:

$$S_{ij} = 0.5\left(\frac{\partial U_i}{\partial x_j} + \frac{\partial U_j}{\partial x_i}\right)$$

And

$$\nu_t = C_\mu \overline{v^2}\, max\left(\frac{k}{\varepsilon}, 6\sqrt{\frac{\nu}{\varepsilon}}\right) \tag{6}$$

To close the system of equations obtained (Eqs. (1) to (5)), the turbulence model $v^2 - f$ of Hanjalic *et al.* (2004) is used. For this model, the transport equations of turbulent quantities are:

$$\frac{Dk}{D\tau} = P_k - \varepsilon + \frac{\partial}{\partial x_j}\left[\left(\nu + \frac{\nu_t}{\sigma_k}\right)\frac{\partial k}{\partial x_j}\right] \tag{7}$$

$$\frac{D\varepsilon}{D\tau} = \frac{C_{\varepsilon 1}P_k - C_{\varepsilon 2}\varepsilon}{T} + \frac{\partial}{\partial x_j}\left[\left(\nu + \frac{\nu_t}{\sigma_\varepsilon}\right)\frac{\partial \varepsilon}{\partial x_j}\right] \tag{8}$$

$$\frac{Dg}{D\tau} = f - \overline{v^2}\frac{P_k}{k^2} + \frac{\partial}{\partial x_j}\left[\left(\nu + \frac{\nu_t}{\sigma_g}\right)\frac{\partial g}{\partial x_j}\right] \tag{9}$$

$$-L^2\Delta f + f = \frac{1}{T}\left(\mathrm{C}_1 + \mathrm{C}_2\frac{P_k}{\varepsilon}\right)\left(\frac{2}{3} - \frac{\overline{v^2}}{k}\right) \tag{10}$$

with $g = \frac{\overline{v^2}}{k}$, $L = C_L max\left[\frac{k^{\frac{3}{2}}}{\varepsilon}, C_\eta\left(\frac{\nu^3}{\varepsilon}\right)^{\frac{1}{4}}\right]$,

$$T = max\left[\frac{k}{\varepsilon}, C_T\left(\frac{\nu}{\varepsilon}\right)^{\frac{1}{2}}\right], C_{\varepsilon 1} = 1.4\left(1 + 0.012\frac{k}{\overline{v^2}}\right) \quad (11)$$

the model constants are grouped in table 1.

Table 1. Constants of the turbulence model $v^2 - f$ (Hanjalic *et al.* (2004))

C_1	C_2	$C_{\varepsilon 2}$	σ_k	σ_ε
0.4	0.65	1.9	1	1.3
σ_{v^2}	C_L	C_η	C_T	C_μ
1.2	0.36	85	6	0.22

The boundary conditions for the mean dimensionless quantities are as follows.

- For the vertical walls:

$$U_i^*(0,Y) = U_i^*(1,Y) = 0,\ \theta(0,Y) = \gamma_1\left(\frac{Y}{A} - 0.5\right) + 1$$

And

$$\theta(1,Y) = \gamma_2(Y/A - 0.5) \quad (12)$$

- For the horizontal walls:

$$\mathrm{U_i^*(X,0) = U_i^*(X,A) = 0, (\partial\theta/\partial Y)_{Y=0} = (\partial\theta/\partial Y)_{Y=A} = 0} \quad (13)$$

- For turbulent quantities, on all solid walls:

$$k = g = 0,\ \varepsilon = 2\nu \lim_{y_n \to 0} k/y_n^2,$$

and

$$\lim_{y_n \to 0} f = -10\nu \lim_{y_n \to 0} \overline{v^2}/(k y_n^2) \quad (14)$$

y_n is the distance to the nearest wall.

The dimensionless variables are expressed as follows:

$$U_i^* = \frac{U_i L}{\alpha}, \theta(Y) = \frac{T(y) - T_c}{T_h - T_c}, X = \frac{x}{L}, Y = \frac{y}{L}, \tau^* = \alpha\frac{\tau}{L^2} \quad (15)$$

The local and average Nusselt numbers on the vertical walls are given by :

$$Nu_{CL} = -\partial\theta/\partial n$$

And

$$Nu_C = \frac{1}{A}\int_0^A Nu_{CL} dY \quad (16)$$

where n denotes the normal direction of the considered vertical wall.

The stream (ψ) and heat (Π) functions can be expressed so that the Eqs. (1) and (3) are automatically satisfied (Kimura and Bejan 1983; Costa 2003). For a two-dimensional flow:

$$\partial[\psi \text{ or } \Pi]/\partial X_{j\neq i} = sign(j-i)\left[(U_i^* \text{or} U_i^*\theta) - \partial\,\theta/\partial X_i + \overline{u_i^* t^*}\right] \quad (17)$$

The signum function $Sign(j-i)$is equal to 1 if $j > i$ and -1 otherwise, and $\overline{u_i^* t^*} = \rho\, C_p L/k_t \Delta T\, \overline{u_\iota(t - T_0)}$.

Since the function Π is defined through its first derivatives, we take $\Pi(0,0) = 0$ as an arbitrary reference of Π.

On solid walls $\psi = 0$, while the boundary conditions imposed on Π are:

Vertical walls $i = 1$ or $2 : \partial\Pi/\partial X = \gamma_i/A$.

Horizontal walls :

$$\partial\Pi/\partial X = 0 \quad (18)$$

3. NUMERICAL PROCEDURE AND VALIDATION

The governing equations of the problem under study are discretized by the finite volume method and then solved by using the SIMPLE algorithm (Patankar (1980)). These equations are solved in transient regime, until reaching the steady state, with a dimensionless time step of 5×10^{-6} . The convergence of computations is considered to be achieved if at any node (i,j) of the grid, there are between two successive iterations $max_{ij}\left|(\phi_{ij}^n - \phi_{ij}^{n-1})/\phi_{ij}^n\right| \leq 10^{-6}$ for all the variables $(U, \theta, P, k, \varepsilon, \overline{v^2}$, and $f)$.

A non-uniform mesh was generated by using the sinusoidal functions $X(i) = 0.5(1 - cos(\pi(i-1)/(n_x - 1)))$ and $Y(j) = 0.5A(1 - cos(\pi(j-1)/(n_y - 1)))$, where n_x and n_y are the number of nodes (i,j) considered in the horizontal and vertical directions, respectively. The effect of the mesh size on the result is presented in table 2 for the extreme case corresponding to $Ra_m = 10^6$ and $A = 80$. As shown in Table 2, for the considered situations, a non-uniform grid of 60×160 is a good compromise between the accuracy of the results and the computing time. In fact, the maximum difference with the results obtained for a mesh of 80×175 does not exceed 0.94% (for ψ_{max} in case (II, $\gamma = 1$)). Note that the results corresponding to cases (II, $\gamma = 1$) and (IV, $\gamma = -1$ or 1) are not presented in table 2 because they are identical to those of cases (II, $\gamma = -1$) and (III, $\gamma = -1$ or 1), respectively.

The developed numerical code has been widely tested by comparing its results with those of close works of the literature on turbulent natural convection (El Moutaouakil *et al.* (2014a)). The validations presented in this work are done with the experimental results (Betts and Bokhari (2000)), obtained on a differentially heated vertical cavity with uniform temperatures ($\gamma = 0$), $A = 28.68$ and $Ra_m = 1.43 \times 10^6$. Figs. 2a and 2b show comparisons on the average temperature of the air and the local Nusselt number on the hot wall at different heights of the cavity. As one can see, in general, there is a good agreement between the numerical and experimental results. By integrating $Nu_{CL1}(Y)$ calculated by the numerical code, we get an average Nusselt number Nu_{C1} which is only at 1% of that provided by Betts and Bokhari (2000).

Table 2 Effect of mesh size for $Ra_m = 10^6$ and $A = 80$

		ψ_{max}			$k_{max} \times 10^{-5}$			Nu_C		
Case	γ	50×145	60×160	70×175	50×145	60×160	80×175	50×145	60×160	80×175
I	-1	188.65	184.74	183.78	1.442	1.476	1.478	5.988	6.046	6.053
	0	174.22	170.03	168.95	1.242	1.249	1.251	6.415	6.435	6.440
	1	158.34	156.23	155.76	1.011	1.049	1.053	6.721	6.753	6.798
II	1	217.73	221.65	223.73	1.932	2.071	2.087	6.825	6.938	6.944
III	-1	205.43	202.23	201.84	1.723	1.745	1.748	6.276	6.355	6.359
	1	192.45	189.32	188.67	1.501	1.528	1.531	6.682	6.705	6.709

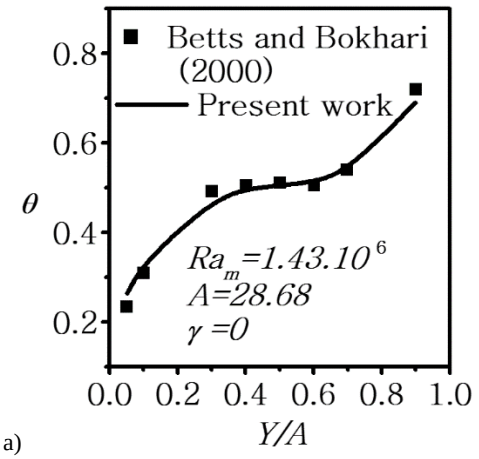

a)

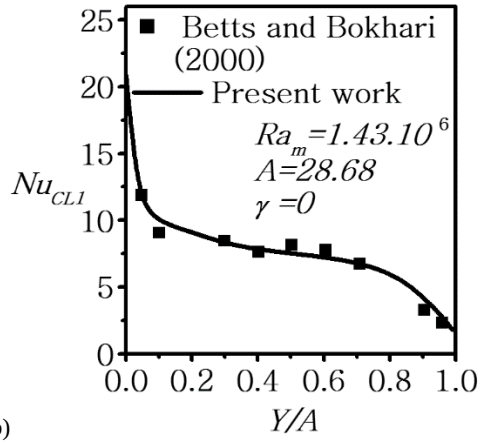

b)

Fig. 2. Validation of the numerical code for $\gamma = 0$, $A = 28.68$, $Ra_m = 1.43\ 10^6$ and $Pr = 0.7$: a) average air temperature and b) local Nusselt number on the hot wall.

4. RESULTS AND DISCUSSION

The flow structure and convective heat transfer depend on local quantities $\theta_m(Y)$ and $Ra(Y)$, which are functions of the controlling parameters Ra_m, A and γ. Note that the classical situation ($\gamma_1 = \gamma_2 = \gamma = 0$) is common to all the considered cases and it is taken as a reference.

The dynamic and thermal fields in a very tall cavity ($A = 80$) are simple while for a moderate aspect ratio ($A = 10$) they are more complex. For this reason, the results corresponding to $A = 80$ are often presented before those of $A = 10$.

4.1. Case I ($\gamma_1 = \gamma_2 = \gamma$) : Effect of $\theta_m(Y)$

For case I ($\gamma_1 = \gamma_2 = \gamma$), Figs. 3a to 3d show the effect of $\theta_m(Y)$ on the dynamic and thermal fields for $Ra_m = 10^6$ and different values of A ($A = 10$ and 80) and γ ($\gamma = -1, 0$ and 1). While the variations of the local Nusselt numbers along the active walls are represented in Figs. 4a and 4b.

Figures 3a and 3b show that ψ_{max} and k_{max} increase with A but decrease with γ. However, their respective positions $Y_{\psi max}$ and Y_{kmax} are always located at mid-height of the cavity. Overall, for a given combination of the controlling parameters Ra_m, A and γ, the flow structure is symmetrical with respect to the cavity centre. For $A = 80$ and all values of γ, the flow structure consists of a single cell rotating in clockwise direction and it is parallel to the active walls in the central part of the cavity. By cons for $A = 10$, the flow structure is no longer simple and change significantly with γ. Thus for $\gamma = -1$, two small cells rotating in counter-clockwise direction appear in the top left and bottom right corners because in these zones the air temperature is higher and lower than that of the hot and cold walls, respectively (Fig. 3c). Passing from $\gamma = -1$ to $\gamma = 1$, the values of ψ_{max} (k_{max}) decrease by approximately 60% (91%) for $A = 10$ and 15% (29%) for $A = 80$. Thus, the profile of $\theta_m(Y)$ has more influence on the flow when the aspect ratio of the cavity is low.

The isolines of turbulent kinetic energy (iso-k) are strongly influenced by the aspect ratio of the cavity, especially for $\gamma = 1$. For $A = 80$ and all the values of γ, the intensity of the fluctuations is important in the core region of the cavity. This is due to the interaction between the vertical boundary layers in the central part of the cavity. Along the horizontal median $Y = A/2$, $k(X, Y = 0.5A)$ is maximum at $X = 0.5$ then decreases rapidly to vanish at $X = 0$ and 1(Eq. (14)). When $A = 10$, the maximum of $k(X, Y = 0.5A)$ is located at $X = 0.5$ if $\gamma \leq 0$, while it is close to the active walls if $\gamma = 1$, indicating that the turbulent boundary layers along the active walls are distinct. Thus, if $A = 10$ and $\gamma = 1$, the flow is practically laminar in the central region of the cavity due to the thermal stratification in this zone ($\theta_m(Y)$ is increasing). Indeed, when passing from A = 10 to A = 80 or from $\gamma = 1$ to -1, the intensification of the fluctuations observed in the

central part of the cavity is due to the reduction of the vertical thermal stratification in the cavity.

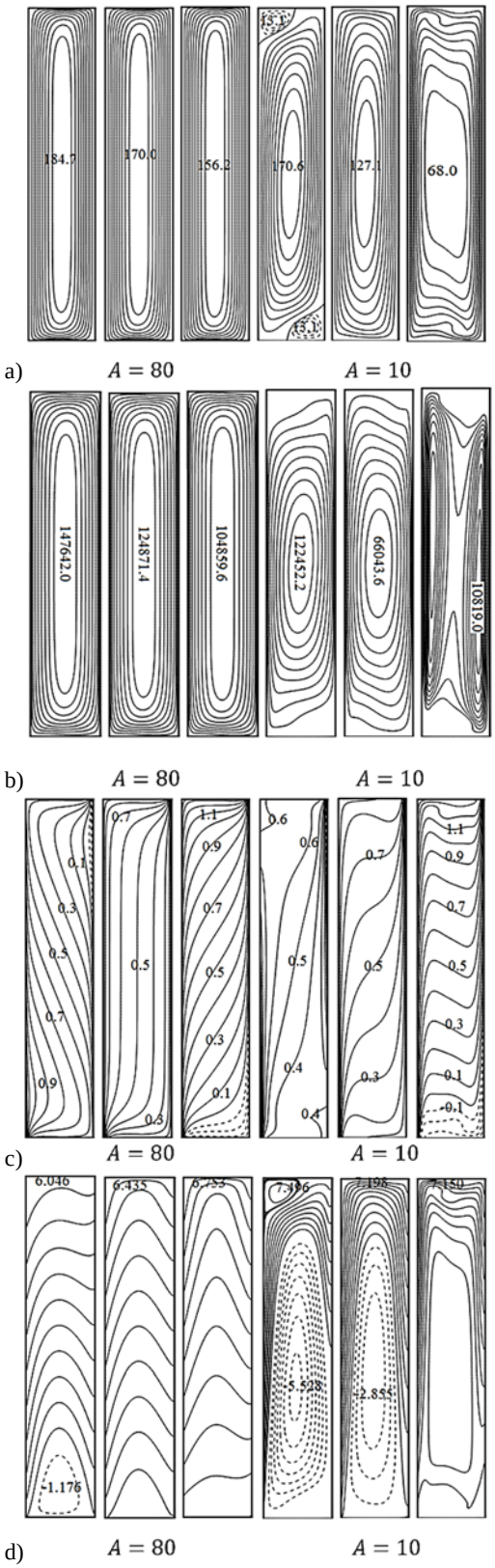

Fig. 3. Isolines for case I with $Ra_m = 10^6$, $\gamma = -1, 0, 1$ (left to right), $A = 80$ and $A = 10$: a) streamlines, b) iso-k, c) isotherms and d) heatlines.

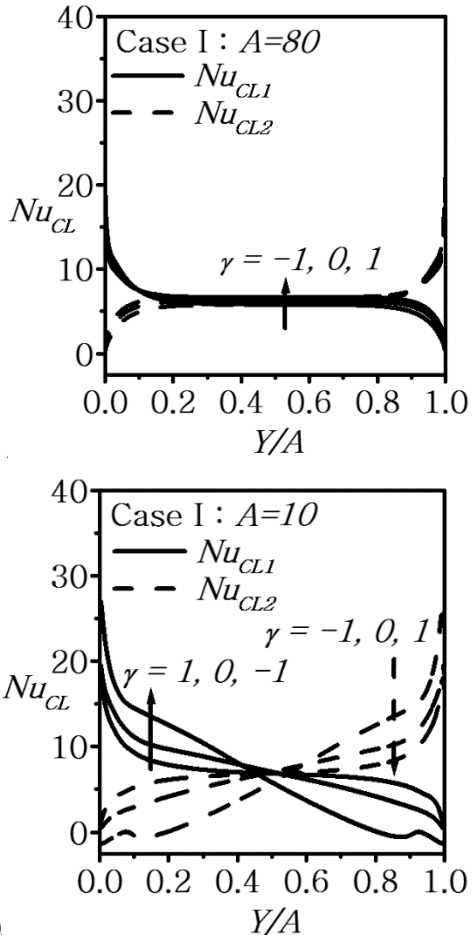

Fig. 4. Local Nusselt number along the active walls for case I with $Ra_m = 10^6$ and different values of γ: a) $A = 80$ and b) $A = 10$.

For $A = 80$ and $\gamma = 0$, Fig. 3c shows that in the central part of the cavity, the isotherms are practically parallel to the active walls of a differentially heated cavity with uniform temperatures. This indicates that the flow is one-dimensional in this zone. When $\gamma \neq 0$, the isotherms are always parallel to each other, but showing a two-dimensional convective heat transfer in the core region of the cavity. Thus, around the middle of the cavity, the fluid temperature $\theta(X = 0.5, Y)$ has a decreasing linear profile, uniform or increasing if $\gamma = -1, 0$ or 1, respectively. However, close to the adiabatic walls, the horizontal flow is intense because there is a high thermal stratification regardless of the value of γ. This significant change observed on the isotherms, when switching from $\gamma = 0$ to $\gamma = -1$ or 1, is due to the evolution of the average temperature $\theta_m(Y)$ with the height of the cavity.

For $A = 10$, the isotherms always have a two-dimensional aspect, even for $\gamma = 0$ (Fig. 3c). This is due to the effect of the horizontal walls which extends to the core region of the cavity. When $\theta_m(Y)$ is uniform or decreasing ($\gamma = 0$ or -1), the isotherms show that the convective heat transfers vary with Y and are especially important at the bottom and top parts of the hot and cold walls, respectively. Note also that when $\gamma = -1$, the top

(bottom) part of the hot (cold) wall has a temperature lower (higher) than that of the surrounding fluid (Fig. 3 c). For $\gamma = 1$, except the upper and lower parts of the active walls, the isotherms show that the local convective heat transfers are almost uniform and similar on the hot and cold walls.

Figure 3d shows, for a very tall cavity ($A = 80$) and a given γ, that a heatline leaving the hot wall reaches directly the cold wall at a height slightly above that of the starting point. In addition, these heatlines are quite well distributed along the active walls, which indicates that the heat is supplied (evacuated) by the hot (cold) wall in an almost uniform manner, except near the adiabatic walls. For $A = 10$, the heat recirculation cells occupy a significant portion of the cavity but their intensities decrease quickly with γ due to the increase of the thermal stratification. For $\gamma = -1$, the heatlines show that the heat given off by the hot wall is mostly transported by the fluid to the upper part of the cold wall while the rest of this heat is provided by natural convection to the upper end of the same wall, because it is relatively cold. Indeed, some heatlines start from a part of the hot wall and terminate at its upper end, because the temperature profile along the wall is decreasing. Note also for $\gamma = -1$ that the lower part of the cold wall heats the surrounding air, without that this heat reaches directly some parts of the active walls. When the temperature of the active walls are uniform ($\gamma = 0$), all the heat provided by the hot wall is transported by the fluid to the cold wall. The density of heatines reaching the cold wall increases with the height, which shows that heat is mainly removed by the upper part of the cold wall. When $\gamma = 1$, the heatlines show that, despite the fact that the hot wall temperature is increasing, the heat removed by the cold wall comes mainly from the lower part of the hot wall due to the thermal saturation of the fluid.

Figures 4a and 4b, show that when $A = 10$ and $\gamma = 1$ or $A = 80$ and all the values of γ, the local Nusselt numbers $Nu_{CL1}(Y)$ and $Nu_{CL2}(Y,\gamma) \approx Nu_{CL1}(A-Y,\gamma)$ are virtually uniform on almost the all height of the active walls. This result was explained by the nearly uniform distribution of heatlines on most of the height of the active walls (Fig. 3d). However, at the top and bottom ends of the active walls, the local Nusselt numbers have significant gradients. As shown by the heatlines, the values of $Nu_{CL1}(Y)$ and $Nu_{CL2}(Y)$ are high (low) at the bottom (top) and top (bottom) of the hot and cold walls, respectively. For the other situations of case I ($A = 10$ and $\gamma \leq 0$), $Nu_{CL1}(Y)$ and $Nu_{CL2}(Y)$ are respectively decreasing and increasing throughout the active walls. As previously explained by the heatlines for $A = 10$, $Nu_{CL1}(Y)$ and $Nu_{CL2}(Y)$ are negative at the top and bottom of the hot and cold walls, respectively.

4.2. Case II ($\gamma_1 = -\gamma_2 = \gamma$) : Effect of Ra(Y)

Figures 5a to 5d, show for $A = 80$ and 10, the streamlines, iso-k, isotherms and heatlines obtained for case II with $Ra_m = 10^6$ and $\gamma = -1$ or 1. The isolines of the classical case ($\gamma = 0$) are given in Fig. 3. Figs. 5a to 5c, show that the isolines of the quantities ψ, θ and k corresponding to $\gamma = 1$ are deductible, by symmetry with respect to the point $X = Y/A = 0.5$, from those obtained for $\gamma = -1$. This is due to the differences between the temperatures of the active walls, which are also symmetrical with respect to the cavity centre. However, the heatlines (Fig. 5c) are not symmetrical because they depend on the chosen origin for the heat function.

Figures 5a and 5b show that when $Ra(Y)$ is not uniform, the flow is no longer symmetrical about the center of the cavity and this for all values of A, Ra_m and $\gamma \neq 0$. However, since $\theta_m(Y)$ is constant ($\theta_m(Y) = 0.5$), the maximum values ψ_{max} and k_{max} (highest values for $A = 80$) depend only on $|\gamma| \neq 0$. By cons, for a given Ra_m, their positions $Y_{\psi max}$ and Y_{kmax} are highly influenced by A and the imposed profile of $Ra(Y)$. Thus, when $Ra(Y)$ is decreasing ($\gamma = -1$), the positions $Y_{\psi max}$ and Y_{kmax} are located below $Y = 0.5A$ and inversely if $Ra(Y)$ is increasing ($\gamma = 1$). For $A = 80$, these two positions are close to the lower ($\gamma = -1$) or upper ($\gamma = 1$) horizontal walls. For $A = 10$, the passive walls have more effect on the fluid flow, resulting in positions $Y_{\psi max}$ and Y_{kmax}, which are more closer to the centre of the cavity where $Ra(Y) = Ra_m$. Thus, for $A = 10$, the values of ψ_{max} and k_{max} obtained for case II ($\gamma \neq 0$) are similar to those found for the classical case ($\gamma = 0$ and $Ra(Y) = Ra_m$). By cons, for $A = 80$, these quantities are much larger, which shows that $Ra(Y)$ has more influence on the dynamic and fluctuating fields in a cavity with a high value of A. Note that when $\gamma = -1$ ($\gamma = 1$), the fluid is almost motionless at the top (bottom) of the cavity, especially if A is high, while for $A = 10$, there is a single small counterclockwise convective cell in the top left (bottom right) corner.

Concerning the isotherms (Fig. 5c), for $\gamma = -1$ there is important temperature gradients in the lower part of the cavity where $Ra(Y = 0) = 2Ra_m$. In the upper part of the cavity, the fluid has virtually a uniform dimensionless temperature (around 0.6) for all values of A because $Ra(Y \to A) \approx 0$.

According to the density of isotherms, and as expected, the local convective transfers are especially important on the lower parts of the hot and cold walls because their temperatures are decreasing and increasing with height, respectively. For $\gamma = 1$, we have opposite situations because the temperature of the hot and cold walls increases and decreases with height, respectively.

Figure 5d shows that for $A = 80$, $\gamma = -1$ and 1, the heatlines have similar shapes. But since $Ra(Y)$ varies, their density decreases ($\gamma = -1$) or increases ($\gamma = 1$) with Y, indicating that, in general, the local heat transfer decreases or increases along the hot wall for $\gamma = -1$ or 1, respectively.

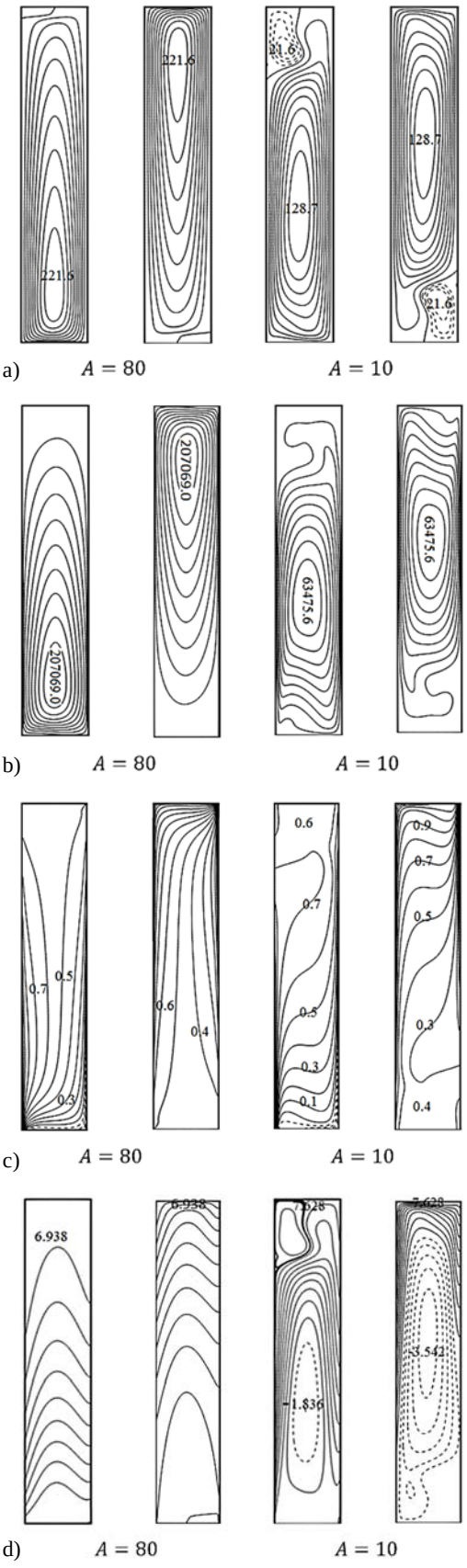

Fig. 5. Isolines for case II with $Ra_m = 10^6$, $\gamma = -1, 1$ (left, right), $A = 80$ and $A = 10$: a) streamlines, b) iso-k, c) isotherms and d) heatlines.

For $A = 10$ and $\gamma = -1$, the heatlines are highly inclined and dense near the vertical walls of the cavity indicating that the convective heat transfer on the active walls is important. Since $\theta_1(Y)$ is decreasing, it is noted again that the heat provided by the hot wall comes mainly from its lower part. A part of this heat is recovered by its top end, which is relatively colder, while the rest is removed by almost the entire cold wall. For $\gamma = 1$, the heat exchanges are mainly between the upper parts of the hot and cold walls, since they correspond respectively to the hottest and coldest portions of the active walls. By switching from case I to case II, the intensity of the heat recirculation cells in the core region of the cavity becomes slightly lower if $\gamma = -1$ and higher if $\gamma = 1$. This is due to the fact that if $\gamma = -1$, the fluid heats almost all the cold wall because $\theta_2(Y)$ is increasing with Y.

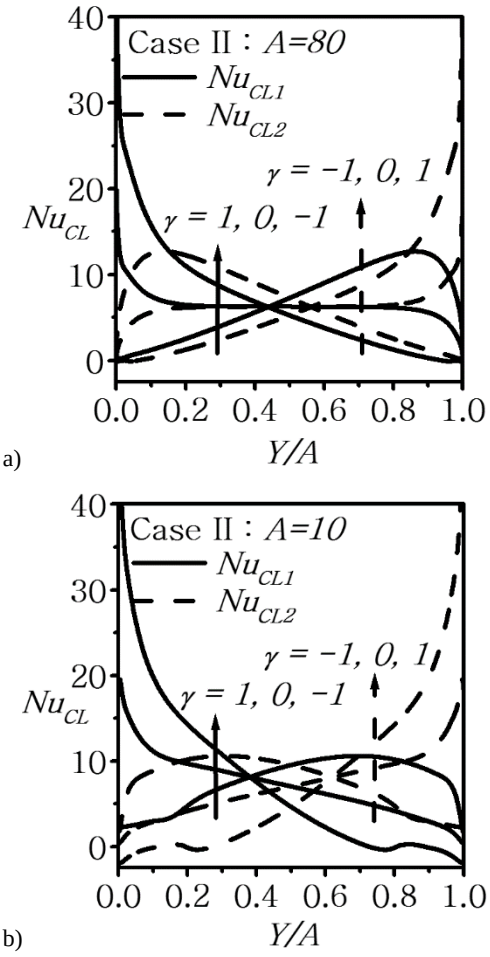

Fig. 6. local Nusselt number along the active walls for case II with $Ra_m = 10^6$ and different values of γ: a) $A = 80$ and b) $A = 10$.

Figures 6a and 6b show that, because of the variation of the local Rayleigh number, the profiles of $Nu_{CL1}(Y,\gamma)$ and $Nu_{CL2}(Y,\gamma)$ undergo significant changes compared to the case I. As explained by the heatlines, the local convective heat transfer decreases rapidly along the hot wall when $\gamma = -1$ and becomes virtually nil if $A = 80$ or negative if $A =$

10 at the top end of the wall. However, unlike case I, the local Nusselt number also decreases on the entire upper half of the cold wall, because $T_2(Y)$ increases with Y. Conversely, when $\gamma = 1$, the local Nusselt numbers increase practically along the two vertical walls of the cavity. With $\gamma = 0$, the local Nusselt numbers along the active walls are always between those calculated for $\gamma = -1$ and $\gamma = 1$. The analysis of the results of case II, showed that for given values of $Ra_m, A,\ \gamma$ and Y, the local Nusselt numbers on the two active walls of the cavity are related by:

$$Nu_{CL2}(Y,\gamma) \approx Nu_{CL1}(A-Y,-\gamma) \quad (19)$$

4.3. Cases III ($\gamma_i = \delta_{i2}\gamma$) and IV ($\gamma_i = \delta_{i1}\gamma$) : Simultaneous Effect of $Ra(Y)$ and $\theta_m(Y)$

Due to the temperature profiles imposed on the active walls, for a given combination of Ra_m, A and γ, the dynamic and thermal fields of case IV can be deducted from those of case III by symmetry with respect to the center of the cavity. This is well illustrated in Figs. 7a and 7b which show that, for $Ra_m = 10^6$, $\gamma = \pm 1$ and $A = 80$ or 10, the local Nusselt number on the hot (cold) wall of case IV can be deduced from that on the cold (hot) wall of case III, by a simple symmetry with respect to $X = Y/A = 0.5$. This is also valid for the classical case ($\gamma = 0$), which was presented and discussed before. Thus, we have just to apply the following relationship to deduce the local Nusselt number of case IV from that of case III and vice versa :

$$Nu_{CL1\text{ or }2}(\mathrm{IV},Y,\gamma) \approx Nu_{CL2\text{ or }1}(\mathrm{III},A-Y,\gamma) \quad (20)$$

For each case III or IV with a given combination of the values of Ra_m, A and γ, the dynamic and thermal fields are no longer symmetrical with respect to the center of the cavity, because $Ra(Y)$ is not uniform as in case I. Also, these fields are no longer symmetrical about the center of the cavity for two opposite values of γ, because $\theta_m(Y)$ is not uniform as in case II. Thus, in cases III and IV, $Ra(Y)$ and $\theta_m(Y)$ vary simultaneously, which gives dynamic and thermal fields that depend significantly on γ, for given values of Ra_m and A. These observations motivated us to look for a relationship between the dynamic and thermal fields of cases III and IV and those of cases I and II which depend only on $\theta_m(Y)$ and $Ra(Y)$, respectively. Detailed analysis of these fields for different values of Ra_m, A and γ, has shown that it is possible to approximate all the local quantities of case (III, γ) by averaging those of cases (I, γ) and (II,$-\gamma$). Subsequently, the local quantities of the case IV may be deducted from those of cases III by symmetry relative to the center of the cavity.

This approach provides an excellent agreement between the local quantities at any point of a cavity with large value of A ($A = 80$), whereas if A is low ($A = 10$), differences are observed especially near the adiabatic walls. However, if one is particularly interested in the local heat transfer, it can be seen that the isotherms (Fig. 8) of case (III, γ) for $Ra_m = 10^6$, obtained directly or by combining the results of cases (I, γ) and (II,$-\gamma$) are generally in good agreement, even for $A = 10$ at the level of active walls. Thus, for a given combination of Ra_m, A and γ, the local Nusselt numbers along the active walls of case III are deducted from those on the vertical walls of cases I and II from:

$$Nu_{CL1\text{ or }2}(\mathrm{III},Y,\gamma) \approx 0.5\left(Nu_{CL1\text{ or }2}(\mathrm{I},Y,\gamma) + Nu_{CL1\text{ or }2}(\mathrm{II},Y,-\gamma)\right) \approx 0.5\left(Nu_{CL2\text{ or }1}(\mathrm{I},A-Y,\gamma) + Nu_{CL2\text{ or }1}(\mathrm{II},A-Y,\gamma)\right) \quad (21)$$

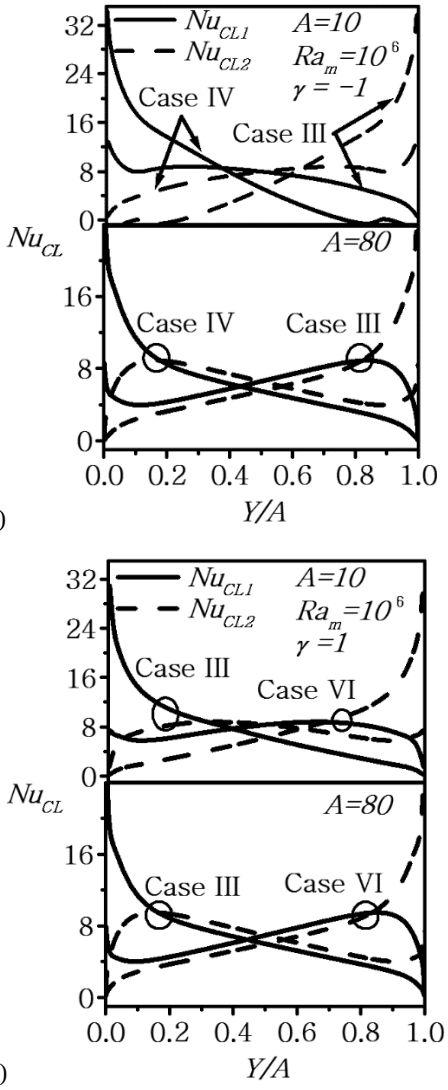

Fig. 7. Local Nusselt number along the active walls for cases III and IV with $Ra_m = 10^6$, $A = 80$ and $A = 10$: a) $\gamma = -1$ and (b) $\gamma = 1$.

For $Ra_m = 10^6$ and $\gamma = -1$ or 1, the local Nusselt numbers of case III and those calculated from Eq. (21) are compared in Figs. 9a and 9b for $A = 80$ and 10, respectively. As shown, Eq. (21) is fairly accurate especially in the central part of the cavity where the effects of the horizontal walls are negligible. Therefore, Eq. (21) is even more precise than the aspect ratio of the cavity is high. Indeed, the highest average deviation is 4.15% and it has been recorded on the hot wall when $Ra_m = 10^6$, $A = 10$ and $\gamma = 1$.

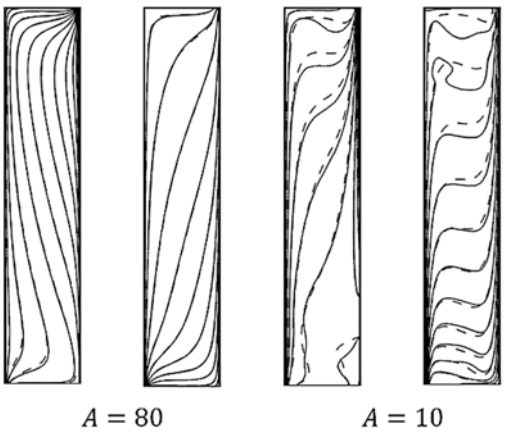

Fig. 8. Comparison of isotherms of case (III, γ) (——) and those deduced from cases (I, γ) and (II,– γ) (- - -) for $Ra_m = 10^6$, $\gamma = -1$, 1 (left, right), $A = 80$ and $A = 10$.

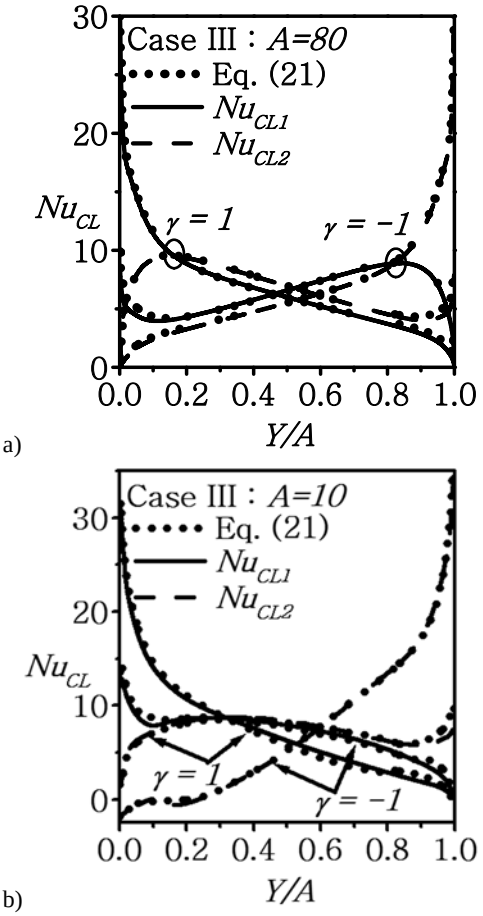

Fig. 9. Comparison of local Nusselt numbers of case III calculated directly and by Eq. (21) for $Ra_m = 10^6$, $\gamma = -1$ and 1: (a) $A = 80$, and (b) $A = 10$.

To calculate the local Nusselt numbers along the active walls of case IV, it suffices to apply Eq. (20).

4.4. Average Heat Transfer

Average heat transfers are analyzed, as a function of Ra_m and A, for each case and the considered values of γ. The evolutions of average Nusselt numbers $Nu_C(\mathrm{I},\gamma)$ and $Nu_C(\mathrm{II},\gamma)$ as a function of Ra_m ($5 \times 10^4 \leq Ra_m \leq 10^6$) are presented for $A = 10$ and 80 in Figs. 10a and 10b. On a logarithmic scale, obtained profiles are straight lines with a slope of about 1/3, except for case $(\mathrm{I}, \gamma = 1)$ with $A = 10$, for which it is about 0.26 because the flow is laminar over a large part of the cavity. For case II, the average Nusselt number depends on $|\gamma|$ because two opposite slopes lead to dynamic and thermal fields that are symmetrical with respect to the center $X = Y/A = 0.5$.

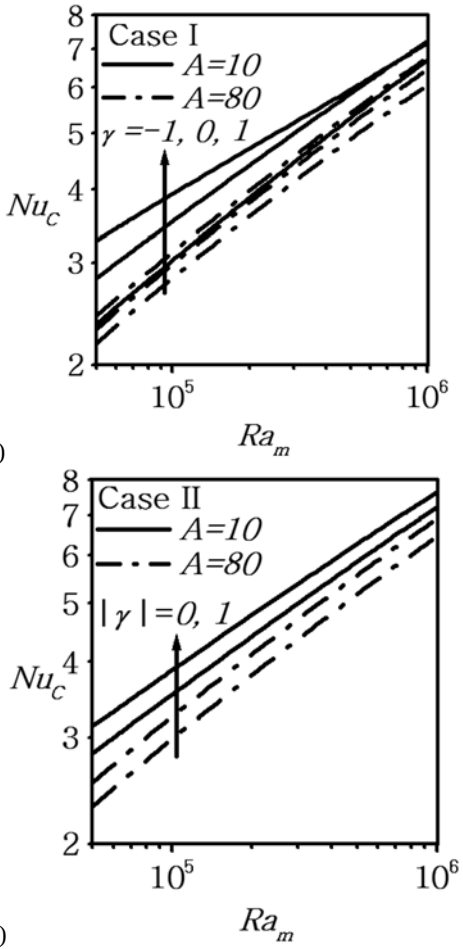

Fig. 10. Evolution of the average Nusselt number as a function of Ra_m for various values of A and γ: (a) case I, and (b) case II.

For cases I and II, Figs. 10a and 10b show that according to the temperature profiles of $T_1(Y)$ and $T_2(Y)$, the heat transfer can be significantly enhanced (case $(\mathrm{I}, \gamma > 0)$ and case $(\mathrm{II}, |\gamma| \neq 0)$) or reduced (case $(\mathrm{I}, \gamma < 0)$) compared to the classical case ($\gamma = 0$). The maximum increase found for case $(\mathrm{I}, \gamma = 1)$ (case $(\mathrm{II}, |\gamma| = 1)$) is about 15.8 % (10.9%) and 5.3% (9.6%) for $A = 10$ and $A = 80$, respectively. Therefore, linear temperature profiles have an effect on the average heat transfer that is inversely proportional to the aspect ratio of the cavity. However, for a given value of A, mean Nusselt numbers of case I if A is low $(A = 10)$ are more important than those of case II if A is high $(A = 80)$. This has been previously explained by the fact that the effects of the parameters $\theta_m(Y)$ and $Ra(Y)$ are more important for $A = 10$ and 80, respectively.

Table 3. Coefficients: (a) a_{ij} (Eq. (23)) and (b) α and β (Eq. (24))

a)

	i/j	1	2	3	4
Classical case ($\gamma = 0$)	1	0.12512	22.12195	0.94432	-0.00005
	2	1.57514	5.56569	-0.30674	-0.00045
Case (I, $\gamma = -1$)	1	0.86371	6.62434	0.85892	0.00056
	2	-0.96743	10.11186	0.16079	-0.00074
Case (I, $\gamma = 1$)	1	-2.0582	4.21272	1.23149	-0.00093
	2	3.63708	8.15091	-1.38671	-0.00062
Case (II, $\lvert\gamma\rvert = 1$)	1	0.12223	31.1107	0.95851	0.00003
	2	2.51899	5.70512	-0.47969	-0.00024

b)

	$\gamma = 0$	Case (I, $\gamma = -1$)	Case (I, $\gamma = 1$)	Case (II, $\lvert\gamma\rvert = 1$)
α	0.095308	0.05429	0.19706	0.124406
β	0.31352	0.34897	0.25982	0.29838

In Fig. 11, average Nusselt numbers $Nu_C(\text{III},\gamma) \approx Nu_C(\text{IV},\gamma)$ calculated numerically and from the integration of Eq. (21), are compared for different values of γ and A. First, note the excellent precision of Eq. (21) that provides average Nusselt numbers with a maximum deviation of 1.8% compared with those computed directly by the simulation code. For given values of Ra_m and A, the average Nusselt number of case III or IV is between that of cases I and II. Compared to the classical case ($\gamma = 0$), the heat transfers can be improved in cases III or IV only if the cold or hot temperatures are increasing ($\gamma = 1$), respectively. This is due to the effects of $\theta_m(Y)$ and $Ra(Y)$, which simultaneously contribute to the increase of the average Nusselt numbers at the level of the active walls. However, for $\gamma = -1$, the opposite occurs because $\theta_m(Y)$ and $Ra(Y)$ have opposing effects. Indeed, when the temperature decreases with Y, $\theta_m(Y)$ reduces the Nusselt numbers (see case I) while $Ra(Y)$ increases the heat transfers when $\gamma \neq 0$ (see case II).

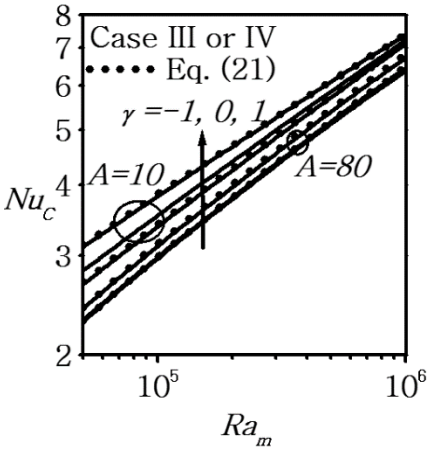

Fig. 11. Comparison of average Nusselt numbers of cases III or VI calculated directly and from Eq. (21) for various values of Ra_m, A and γ.

4.5. Simplified Calculation Procedure for $Nu_C = f(Ra_m, A)$

The computation of average convective heat transfers from the equations of conservation in turbulent regime is complex and laborious. So, for each situation, we tried to develop a simplified procedure, fairly general and accurate, which allows to determine $Nu_C = f(Ra_m, A)$. This procedure is to establish only for cases I and II, because the integration of Eqs. (20) and (21) allows to determine the mean Nusselt numbers of cases III and IV if those of cases I and II are known. To this end, for each γ of cases I and II, we generated by the numerical code a large number of $Nu_C = f(Ra_m, A)$ by varying Ra_m and A from 5×10^4 to 10^6 and from 10 to 80, respectively.

The analysis of the numerical results allowed to establish a precise simplified computing procedure which gives $Nu_C = f(Ra_m, A)$ as a function of $Nu_C(Ra_m, A = 10)$:

$$Nu_C(Ra_\text{m}, A) = f_1(A) Nu_C(Ra_\text{m}, A = 10) + f_2(A) \quad (22)$$

where $f_i(A)$ ($i = 1$ or 2) are two functions that take into account the effect of the aspect ratio A. After several tests, the following empirical expressions have been adopted:

$$f_i(A) = a_{i1} e^{-A/a_{i2}} + a_{i3} + a_{i4} A \quad (23)$$

the coefficients a_{ij} ($i = 1,2$ and $j = 1$ to 4) of Eq. (23) are given in table 3a.

For cases (I,γ) and (II,γ), It was found that the average Nusselt number for $A = 10$ can be calculated accurately from the empirical relationship:

$$Nu_C(Ra_m, A = 10) = \alpha {Ra_m}^{\beta} \quad (24)$$

the coefficients α and β of Eq. (24) are given in table 3b.

For cases I and II, Eqs. (22) to (24) allow estimating

the average Nusselt numbers calculated by detailed simulation with a maximum difference less than 3%, while the average deviation does not exceed 1.8%.

For each combination of values of γ, Ra_m and A, the mean Nusselt numbers of cases III and IV can be estimated with a good accuracy from:

$$Nu_C(\mathrm{III},\gamma) \approx Nu_C(\mathrm{IV},\gamma) \approx 0.5\big(Nu_C(\mathrm{I},\gamma) + Nu_C(\mathrm{II},-\gamma)\big) \quad (25)$$

where $Nu_C(\mathrm{I},\gamma)$ and $Nu_C(\mathrm{II},-\gamma)$ are to be calculated from Eq. (22).

For cases III and IV, Eq. (25) allow estimating the average Nusselt numbers calculated by detailed simulation with a maximum difference less than 4.5%, while the average deviation does not exceed 1.9%.

These minor differences, show that the developed simplified procedure is accurate for all cases treated and each γ ($\gamma = -1, 0$ or -1), despite the wide ranges of Ra_m ($5 \times 10^4 \leq Ra_m \leq 10^6$) and A ($10 \leq A \leq 80$).

5. CONCLUSION

The effects of the slope γ ($\gamma = -1,0$ and 1), the average Rayleigh number Ra_m ($5 \times 10^4 \leq Ra_m \leq 10^6$) and the aspect ratio of the cavity A ($10 \leq A \leq 80$) on the streamlines, isotherms, contours of the turbulent kinetic energy, heatlines, local and average Nusselt numbers have been presented and analyzed. Based on the numerical results found, the following conclusions can be drawn:

- For a given combination of the controlling parameters Ra_m, A and γ, the dynamic and thermal fields in case I are centrosymmetric, while in case II , these are the fields corresponding to the combinations ($Ra_m, A, \gamma \neq 0$) and ($Ra_m, A, -\gamma \neq 0$) which are symmetrical with respect to the center of the cavity. The dynamic and thermal fields obtained in cases III and IV may be deducted by combining those of cases I and II.
- The heatlines show that for a very tall cavity ($A = 80$), in case I the heat is supplied (evacuated) by the hot (cold) wall in an almost uniform manner, except near the adiabatic walls. However, for the other situations and depending on the considered case (I to IV, γ, A), the heat provided (removed) is more important on a given part of the hot (cold) wall and heat recirculation cells occupy a significant portion of cavities with moderate values of A ($A = 10$).
- Compared to the classical situation ($\gamma = 0$), there is improvement of the average heat transfer for cases ($\mathrm{I}, \gamma = 1$) and ($\mathrm{II}, |\gamma| = 1$), while there is a reduction for case ($\mathrm{I}, \gamma = -1$).
- For cases III and IV, the average heat transfers are improved, with respect to the classical situation, if the temperature of the cold or hot wall is increasing. If these temperatures are decreasing, the heat transfer is quite lower.

Finally, for a fast and accurate estimation of the heat transfer through the cavity, a simplified calculation procedure that gives the average Nusselt number as a function of Ra_m and A is exposed for each value of γ and case considered in this work.

REFERENCES

Aksouh, M., A. Mataoui, N. Seghouani and Z. Haddad (2011). Rayleigh Number Effect on the Turbulent Heat Transfer within a Parallelepiped Cavity. *Thermal Sciences* 15(2), 341–356.

Anandalakshmi, R. and T. Basak (2013). Analysis of Natural Convection via Entropy Generation Approach in Porous Rhombic Enclosures for Various Thermal Aspect Ratios. *International Journal of Heat and Mass Transfer* 64(Sep.), 224-244.

Arani, A. A., M. Mahmoodi and S. M. Sebdani (2014). On the Cooling Process of Nanofluid in a Square Enclosure with Linear Temperature Distribution on Left Wall. *Journal of Applied Fluid Mechanics* 7(4), 591-601.

Aswatha, C. J., G. Gangadhara, S. N. Sridhara and K. N. Seetharamu (2011). Effect of Different Thermal Boundary Conditions at Bottom Wall on Natural Convection in Cavities. *Journal of Engineering Science Technology* 6, 109-130.

Aswatha, C. J., G. Gangadhara, S. N. Sridhara and K. N. Seetharamu (2012). Buoyancy Driven Heat Transfer in Cavities Subjected to Thermal Boundary Conditions at Bottom Wall. *Journal of Applied Fluid Mechanics* 5(2), 43-53.

Basak, T., and A. J. Chamkha (2012). Heatline Analysis on Natural Convection for Nanofluids Confined within Square Cavities with Various Thermal Boundary Conditions. *International Journal of Heat and Mass Transfer* 55(21-22), 5526-5543.

Basak, T., D. Ramakrishna, S. Roy, A. Matta and I. Pop (2011). A Comprehensive Heatline Based Approach for Natural Convection Flows in Trapezoidal Enclosures : Effect of Various Walls Heating. *International Journal of Thermal Sciences* 50(8), 1385-1404.

Basak, T., R. Anandalakshmi, and A. K. Singh (2013). Heatline Analysis on Thermal Management with Conjugate Natural Convection in a Square Cavity. *Chemical Engineering Science* 93, 67-90.

Basak, T., S. Roy and A. R. Balakrishnan (2006). Effects of Thermal Boundary Conditions on Natural Convection Flows within a Square Cavity. *International Journal of Heat and Mass Transfer* 49(23-24), 4525-4535.

Basak, T., S. Roy and I. Pop (2009). Heat Flow Analysis for Natural Convection within Trapezoidal Enclosures Based on Heatline Concept. *International Journal of Heat and Mass Transfer* 52(11-12), 2471-2483.

Betts, P. L. and I. H. Bokhari (2000). Experiments of Turbulent Natural Convection in an Enclosed

Tall Cavity. *International Journal of Heat and Fluid Flow* 21(6), 675-683.

Billard, F. (2011). *Development of a Robust Elliptic-Blending Turbulence Model for Near-Wall, Separated and Buoyant Flows*, Ph. D. thesis, the Manchester University, Manchester, England.

Costa, V. A. F. (2003). Unified Streamline, Heatline and Massline Methods for the Visualization of Two-Dimensional Heat and Mass Transfer in Anisotropic Media. *International Journal of Heat and Mass Transfer*, 46(8), 1309-1320.

Deng, Q. H. and J. Chang (2008). Natural Convection in a Rectangular Enclosure with Sinusoidal Temperature Distributions on Both Sidewalls. *Numerical Heat Transfer A* 54(5), 507-524.

El Moutaouakil, L., Z. Zrikem and A. Abdelbaki (2014a). Performance of Various RANS Eddy Viscosity Models for Turbulent Natural Convection in Tall Vertical Cavities. *Heat Mass Transfer* 50(8), 1103-1113.

El Moutaouakil, L., Z. Zrikem and A. Abdelbaki (2014b). Multicellular Convection Flow and Heat Transfer in a Tall Vertical Cavity with Linear Temperature Profile on Both Sidewalls. *Numerical Heat Transfer A* 66(4), 449-470.

El Moutaouakil, L., Z. Zrikem and A. Abdelbaki (2015). Interaction of Surface Radiation with Laminar and Turbulent Natural Convection in Tall Vertical Cavities: Analysis and Heat Transfer Correlations. *Heat Transfer Engineering* 36(17), 1472-1484.

ElSherbiny, S. M., G. D. Raithby and K. G. T. Hollands (1982). Heat Transfer by Natural Convection Across Vertical and Inclined Air Layers. *ASME Journal of Heat Transfer* 104(1), 96-102.

Hanjalic, K., M. Popovac and M. Hadziabdic (2004). A Robust Near-Wall Elliptic-Relaxation Eddy-Viscosity Turbulence Model for CFD. *International Journal of Heat and Fluid Flow* 25(6), 897-901.

Jamai, H., S. O. Fakhreddine and H. Sammouda (2014). Numerical Study of Sinusoidal Temperature in Magneto-Convection, *Journal of Applied Fluid Mechanics* 7(3), 493-502.

Kaluri, R. S., R. Anadalakshmi and T. Basak (2010). Bejan's Heatline Analysis of Natural Convection in Right-Angled Triangular Enclosures : Effect of Aspect Ratio and Thermal Boundary Conditions. *International Journal of Thermal Sciences* 49(9), 1576-1592.

Kimura, S. and A. Bejan (1983). The Heatline Visualization of Convective Heat Transfer. *ASME Journal of Heat Transfer* 105(4), 916-919.

Manz, H. (2003). Numerical Simulation of Heat Transfer by Natural Convection in Cavities of Façade Elements. *Energy and Buildings* 35(3), 305-311.

Omranian, A., T. J. Craft and H. Iacovides (2014). The Computation of Buoyant Flows in Differentially Heated Inclined Cavities. *International Journal of Heat and Mass Transfer* 77, 1-16.

Patankar, S. V. (1980). *Numerical heat transfer and fluid flow*, Hemisphere, Washington, D. C.

Rajani, B. N., A. Kandasamy and S. Majumdar (2012). On the Reliability of Eddy Viscosity Based Turbulence Models in Predicting Turbulent Flow past a Circular Cylinder Using URANS Approach. *Journal of Applied Fluid Mechanics* 5(1), 67-79.

Ramakrishna, D., T. Basak, S. Roy and I. Pop (2012). A Complete Heatline Analysis on Mixed Convection within a Square Cavity : Effects of Thermal Boundary Conditions via Thermal Aspect Ratio. *International Journal of Thermal Sciences* 57, 98-111.

Roy, S. and T. Basak (2005). Finite Element Analysis of Natural Convection Flows in a Square Cavity with Non-Uniformly Heated Wall(s). *International Journal of Engineering Science* 43(8-9), 668-680.

Saeid, N. H. and Y. Yaacob (2006). Natural Convection in a Square Cavity with Spatial Side-Wall Temperature Variation. *Numerical Heat Transfer A* 49(7), 683-697.

Sathiyamoorthy, S., T. Basak, S. Roy and I. Pop (2007). Steady Natural Convection Flows in a Square Cavity with Linearly Heated Side Wall(s). *International Journal of Heat and Mass Transfer* 50(3-4), 766-775.

Wright, J. L. (1996). A Correlation to Quantify Convective Heat Transfer Between Vertical Window Glazings. *ASHRAE Transactions* 106, 940-946.

Xàman, J., G. Alvarez, L. Lira and C. Estrada (2005). Numerical Study of Heat Transfer by Laminar and Turbulent Natural Convection in Tall Cavities of Façade Elements. *Energy and Buildings* 37(7), 787-794.

Yin, S. H., T. Y. Wung and K. Chen (1978). Natural Convection in an Air Layer Enclosed within Rectangular Cavities. *International Journal of Heat and Mass Transfer* 21(3), 307-315.

Zhang, Z., W. Zhang, Z. Zhai and Q. Chan (2007). Evaluation of Various Turbulence Models in Predicting Airflow and Turbulence in Enclosed Environments by CFD : part-2 : Comparison with Experimental Data from Literature. *HVAC&R Research* 13(6), 871-886.

Zhao, Y., W. P. Goss, D. Curcija and J. P. Power (1997). On a New Set of Analytical Correlations for Predicting Convective Heat Transfer in Fenestration Glazing Cavities. *Proceedings of CLIMA 2000* Brussels, 305-316.